




Cite this: *Nanoscale*, 2017, **9**, 9676

The memristive effect as a novelty in drug monitoring†

Ioulia Tzouvadaki, *‡, Nima Aliakbarinodehi,*‡, Giovanni De Micheli and Sandro Carrara

Nanoscale devices exhibiting memristive properties show great potential in a plethora of applications. In this work, memristive nanowires are presented for the first time as ideal candidates for absolutely novel, ultrasensitive, highly specific and selective drug-biosensors, also paving the way for real-time monitoring applications, in coupling with the restoration properties of DNA-aptamers. The hysteretic properties exhibited by the hereby-presented special nanodevices, modified *via* surface treatments, are leveraged along the complete cycle consisting of DNA-aptamer immobilization, target binding, and DNA-aptamer regeneration for successful and effective detection of Tenofovir, an antiviral drug for HIV treatment, in buffer as well as in non-diluted human serum. This results in ultrasensitive, label-free monitoring of the therapeutic compound with a limit of detection of 3.09 pM in buffer and 1.38 nM in full serum. These LODs demonstrate 10 times higher sensitivity for the in-buffer drug detection, and twice better performance for drug sensing in full human serum, ever obtained. The selectivity of the memristive biosensor for Tenofovir detection was verified through both positive and negative controls in full human serum. In addition, the DNA-aptamer regeneration character is portrayed for the first time through a memristive effect, and scanning electron microscopy throws more light on the binding mechanism efficiency through the variation of the nanodevice surface properties at the nanoscale. The results presented in this work demonstrate that the coupling of the memristive effect and aptamer regeneration provides the best ever realized nano-biosensor for drug detection also in full human serum.

Received 21st February 2017,
Accepted 6th June 2017

DOI: 10.1039/c7nr01297g

rsc.li/nanoscale

Introduction

Therapeutic drug monitoring (TDM) is a modern therapeutic approach that proposes to monitor the concentration of drug compounds over time in a patient's circulatory system in order to maintain drug concentrations in plasma or blood within a targeted therapeutic range. This aims at the individualization of the drug dosage regime for optimal efficacy and safety of the treatment.¹ This results in a chemical treatment based on patients' characteristics (genetic profile, age, race, gender, environmental agent, *etc.*), as well as on drug characteristics including pharmacodynamics, pharmacokinetics, drug-drug interactions, adverse effects, *etc.*² As opposed to traditional monitoring technologies usually proposed for TDM, Point-of-Care (PoC) devices will provide a cutting-edge for economical and user-friendly monitoring new systems directly available

to patients too, which would help them to continuously monitor drug concentrations and administrations whenever is required, also at home.

Despite the body of research available about drug detection, innovative ultrasensitive biosensing assays with improved performance in terms of reliability, sensitivity, and detection limit, and the miniaturization capability are still needed, especially targeting the few nM concentration range.

DNA-aptamers are synthetic DNA receptors developed *via* an *in vitro* selection technique (SELEX) to bind specifically and selectively to a particular target. Aptamers are chemically highly stable and retain most of their functionality even after multiple regeneration steps.³ In contrast to antibodies, such a highly repeatable and easy regeneration of aptamers allows for continuous monitoring even upon decreasing target concentrations. These benefits make them ideal candidates for novel biosensor design in continuous diagnostics. In addition, structures like semiconductor nanofabricated wires manifest great potential for the realization of extremely miniaturized bioassays.^{4–7} Thanks to their tunable electron transport properties and the fact that their electrical response is strongly influenced by even minor perturbations, as a consequence of their high surface-to-volume ratio obtained when designed at

Integrated System Laboratory, École Polytechnique Fédérale de Lausanne, 1015 Lausanne, Switzerland. E-mail: ioulia.tzouvadaki@epfl.ch, nima.aliakbarinodehi@epfl.ch, giovanni.demicheli@epfl.ch, sandro.carrara@epfl.ch
†Electronic supplementary information (ESI) available. See DOI: 10.1039/c7nr01297g

‡These authors contributed equally.

the nanoscale, such semiconductor wires offer the possibility for a direct and highly sensitive electrical readout.⁸

Meanwhile, memory effects widely appear in nature,^{9–11} as well as in electronic-based devices where a pronounced hysteresis in the electrical characteristics is a unique fingerprint of the memristive phenomena.^{12,13} Theoretically conceived and presented for the first time by L. Chua in 1971^{14–16} and physically implemented in 2008 by HP laboratory,¹⁷ nanoscale devices exhibiting memristive behavior can be nowadays fabricated from various materials^{18,19} and show immense potential in a plethora of applications. Such nonlinear dynamical memory devices present growing interest also for computation and logic operations,^{20–22} as well as for storage applications.²³ At the same time, implementations in biophysics and temporal dynamics have drawn considerable attention. Nevertheless, so far, the main focus has been on the field of bio-inspired computation and mainly on neuronal systems.^{24–28}

Memristive aptasensors have been proposed for cancer biomarker detection and tested as a proof of concept, and results are published by Tzouvadaki and Jolly *et al.*²⁹ Moreover, we hereby present a new work that opens to a completely new class of memristive aptasensors for continuous monitoring of therapeutic compounds. DNA-aptamer regeneration coupled with the memristive effect is demonstrated for effective drug detection in human serum by the benefit of this kind of memory effect when DNA-aptamers are anchored on the surface of a nanoscale silicon device. The present work actually bridges for the first time ever-reported the memristive effect and the hysteretic electrical properties expressed by nanoscale devices with the DNA-aptamer nature and physical functions. Moreover, successful label-free screening of Tenofovir (TFV), proposed as a drug model in this case of study, is further achieved considering as a starting point this highly controllable DNA-aptamer regeneration character. This ultrasensitive label-free screening of the drug is initially shown in buffer and then efficaciously demonstrated in full human serum. This approach, based on such unique and definitely innovative nanoscale devices, holds great promise for continuous monitoring of drugs in real-time, and may have high impact in the medical practice especially in the field of personalized medicine, which still lacks analytical methods for the continuous monitoring of therapeutic compounds. Furthermore, the suggested approach may pave the way for potential new integrations and multiplexing aspects in diagnostics and personalized medicine.

Experimental

Materials

Amino group terminated TFV-aptamers (5'-aptamer-C6 amino-3') were commercially provided by BasePair Biotechnologies (Pearland, Houston, USA). Human serum, magnesium chloride (MgCl₂), DMSO and PBS (10 mM; pH-7.4) were all purchased from Sigma-Aldrich (Switzerland). PBS buffer was always filtered through 0.2 μm filters before use. Sodium

hydroxide solution (NaOH) was purchased from Sigma Aldrich (Switzerland) and diluted to the concentration of 1 M. Silane (3-glycidyloxypropyl)trimethoxysilane (GPTES) was purchased from Sigma-Aldrich (Switzerland) and used as received. TFV and enzalutamide powders were purchased from Medchemtronica (Stockholm, Sweden) and were dissolved in dimethyl sulfoxide (DMSO) to the concentration of 5 mM as a stock solution, and then they were diluted to the concentration of 100 μM and, subsequently, diluted in sample solutions (buffer or undiluted human serum) to the required concentrations. All other reagents were of analytical grade. All aqueous solutions were prepared using 18.2 MΩ cm ultrapure water with a Pyrogard filter (Millipore, Feltham, UK).

Memristive nano-biosensor fabrication

The nano-biosensor suggested combines the top-down nanofabrication approach for the realization of the memristive wires and bottom-up strategies for the acquisition of the final memristive nano-bio-sensor.

Silicon nanowire devices are fabricated through a top-down fabrication process performed on (100) oriented silicon-on-insulator wafers with a low boron concentration ($N_A \approx 10^{15}$ atoms per cm³). The nanofabrication process can be summarized in two e-beam lithography operations. The first combined with Ni evaporation, liftoff, and annealing processes for obtaining NiSi contact pads for electrical characterization, and, the second for the nanowire definition that are then etched through repeated Deep Reactive Ion Etching cycles (DRIE) of crystalline silicon. Schottky-barrier junctions are formed between the Si and NiSi terminals. With this process, vertically stacked, suspended, silicon nanowire (Si-NW) arrays anchored between two NiSi pillars are achieved.

Gas phase silanization (CVD) was performed on the surface of silicon nanowires in a cleanroom, in order to form an absolutely homogenous layer of GPTES molecules. To this aim, bare silicon nanowires were activated, firstly, by oxygen plasma treatment for 15 minutes (Harrick Oxygen-Plasma, 200 mTorr, 29 W). This bombardment of the surface with high-energy oxygen ions formed a layer of hydroxyl groups on the surface (hydroxylation). Then, activated nanowires were placed in a desiccator under normal vacuum conditions along with 500 μL of the silane-solution for 2 hours. A chemical reaction between hydroxyl groups and methoxy groups on silane molecules in the gas phase formed durable and homogenous binding (covalent bonds) of GPTES across the nanowire surfaces.⁴⁸

The aptamer was developed for specific interaction with TFV. These aptamers were functionalized with the amino group at their 3' terminal to be used as a handle for immobilization. In order to activate the aptamers, they were diluted to the final concentration of 2 μM in 10 mM PBS solution and 1 mM MgCl₂, and then they were unfolded by heating them at 90 °C for 5 minutes and let them to cool down to room temperature (approximately 30 minutes). The silane-coated nanowires (described above) were incubated in this solution of 2 μM TFV-aptamer for 30 minutes. This interval ensures the complete formation of the sensing surface by covalent binding

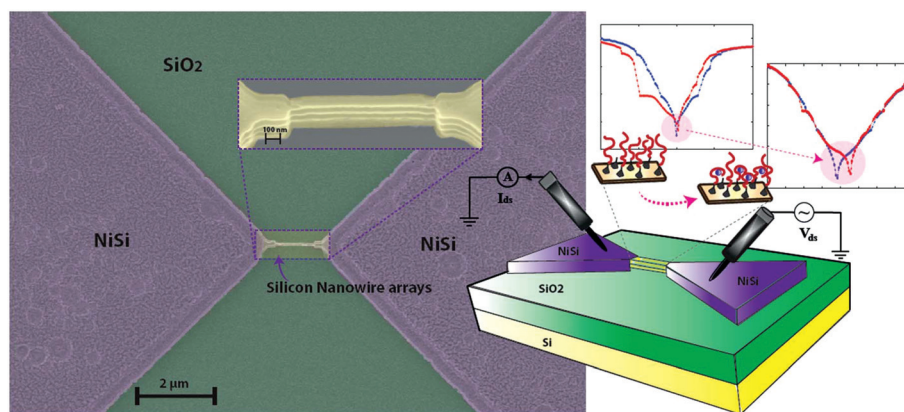


Fig. 1 Schematic representation illustrating the memristive aptasensor and SEM micrograph depicting the Si-NW arrays anchored between the NiSi pads, which serve as electrical contacts of the freestanding memristive nano-device. Schottky-barrier junctions are formed between the Si and NiSi terminals. The position of the current minima for the forward and the backward regime changes after the surface treatment introducing a voltage difference in the semi-logarithmic current to voltage characteristics.

between the amino groups of aptamers and the glycidyl groups of GPTES. After that, nanowire chips were washed with PBS and distilled water to remove any unbound aptamers and salts. At the end, chips were dried with nitrogen gas, and stored at room temperature.

A series of denaturation, pH shocking and refolding was used for surface regeneration (unbind the target from the aptamer and restore the aptamers to their folded and functional form they had before the conformational change): nanowires were excessively washed with deionized water to remove any drug or salts; then, they were incubated in 2 M NaCl solution at 85 °C for 10 minutes in order to denature the aptamers and, thus, unbind the target from the aptamer; they were further immersed in 1 M NaOH solution to give a pH shock to them to eliminate any remaining drug–aptamer binding, followed by deionized-water rinsing; finally they were inserted in 1 mM PBS-MgCl₂ solution at 85 °C for 2 minutes and allowed to cool down for 15 minutes. The last step caused any denatured or collapsed aptamer to be refolded, and thus the sensing surface was functional for new detection.

Electrical and morphological analysis

The electrical characteristics of the nanofabricated memristive structures are acquired using a probe station and contact probe configuration in the semi-logarithmic scale using a Keithley 6430 semiconductor characterization system in a two terminal configuration by double sweeping the source to drain voltage between -2.4 V and $+2.4$ V. The responsive speed for the measurement of each nanodevice is in the range of 1.5–2 minutes. These measurements allow the observation of the changing hysteresis properties of the memristive biosensors as a function of the surface treatment that leads to a charge variation. Electrical characterization performed on wires after the nanofabrication process indicates a hysteretic loop at zero voltage for the forward and the backward regimes of the current. In these devices, the memory effect depends on the charge carrier rearrangement at the nanoscale due to exter-

nal perturbations, such as an applied voltage bias. The hysteresis modification after the surface treatment is studied in terms of voltage difference calculated between the forward and backward current minima of the electrical characteristic curves. All of the measurements were carried out at room temperature, under dry conditions under controlled relative humidity (rH%). It is important to highlight that throughout the present work a stable value for the rH% is maintained to ensure that the observed hysteresis variations directly correspond only to the drug binding reaction. In order to ensure proper control, the rH% was continuously monitored in this work. More specifically, the monitoring was performed using feedback from a Rotronic HC2-C04 Thermo-Hyrometer tool that provides accurate control of rH% of the measurement environment.

In addition to the electrical validation, morphological analysis of the memristive biosensors is carried out using a Scanning Electron Microscope MERLIN, from Zeiss. The imaging is performed at 1.7 kV (Fig. 1 main), 15 kV and stage at 34.9° (inset image Fig. 1) and 1.2 kV (Fig. 3). Due to the top-down nanofabrication process used, the width along the structures is not perfectly homogeneous. However, this can increase the freely available area for DNA aptamer binding, which increases DNA aptamer loading and hence better performance of the biosensors.

Results and discussion

Coupling electrical hysteresis and DNA-aptamer regeneration nature

The regeneration properties of the DNA-aptamers are directly reflected on the biosensor hysteretic electrical response, and expressed through a voltage difference appearing in the semi-logarithmic current to voltage characteristics. The electrical properties of these nanostructures strongly depend on the local environment surrounding the freestanding nanowire,

and on the charge change on the surface of the wire. These charges induce a field effect surrounding the conductive channel in the wire of the memristive device that significantly changes the inside carriers' concentration and consequently affects the whole conductance. Therefore, the hysteresis observed on the device conductance is modified when charged substances are bound to the surface, and the current minima for the forward and the backward regimes appear shifted to different voltage values as shown in Fig. 1.

The whole sensing cycle consisting of aptamer immobilization, target–drug binding, aptamer regeneration, and target–drug re-binding is efficiently, and, for the first time illustrated through the variations of the electrical hysteresis of the memristive nanostructures.

The average hysteretic response of nine independent memristive nanodevices to the consecutive surface treatment steps performed is featured in Fig. 2. All measurements are performed in air under controlled and stable rH%. It is worth noting that after treatment with DNA-aptamers the electrical response of the nanodevices indicates a voltage difference of 116 ± 34 mV. Furthermore, as hypothesized, following the nanodevice exposure to the target drug solution of 100 nM, an increase of the voltage difference occurs as an aftereffect of the drug binding, reaching the value of 156 ± 24 mV indicating an increase of 34.5%. This change is a consequence of the modification in the charge density at the surface of the device due to the introduction of the negatively charged drug molecules.

However, the most promising outcome undoubtedly lies on the electrical response after the regeneration of aptamers that follows the drug binding. Interestingly, it is demonstrated that the voltage difference decreases after the regeneration process to the value of 120 ± 15 mV, and, actually returns at the level that corresponds to the value obtained initially just after the aptamer immobilization on the surface. In order to verify the

nano-biosensor reliability in repeated measures and the capability for further capturing and detecting the target molecules after the aptamer regeneration as well as the biosensor response to a different concentration of the sensing target the very same nano-devices are anew exposed to the drug solution, but, this time, a higher concentration of 1 μ M is introduced. A higher concentration of reagent implies higher charge density and, as expected, the uptake of higher concentration of the drug results in a more pronounced modification of the voltage-gap. In this case, a 100% increased signal is acquired and the voltage difference indicates the value of 240 ± 23 mV that is twice the signal exhibited by DNA-aptamers. It is worth mentioning that the percentage of the signal difference for the hysteresis modification between the two different drug concentrations is estimated to be around 53.8%. Finally, a further regeneration step is carried out to illustrate the nano-biosensors' repeated-regeneration character. It is indeed demonstrated that the voltage difference of 121 ± 39 mV registered after this further regeneration process also coincides with the value achieved initially for the aptamer immobilization on the surface that is also the same as the one obtained after the first regeneration.

This means the biosensor is very reproducibly down to the original value of the voltage-gap after any regeneration process and, therefore, ready for a new measure of the target molecule concentration. The reproducibility of the device after the regeneration, here presented as the percentage differences between the hysteresis modification signals obtained after the initial aptamer immobilization and the two regeneration procedures applied, is around 3.4% and 4.3% for these two regenerations, respectively. These percentages can be considered negligible indeed, also comparing with measurement errors usually obtained in detection on drug binding. Overall, it is worth highlighting that all these findings indicate clear evidence that DNA-aptamer natural characteristics to bind to drugs and related functions may indeed be efficiently transduced by using the memristive phenomena and its electrical hysteretic properties as well, which constitute here a premiere case of evidence.

Effective, label-free, drug screening

Having demonstrated the direct and highly efficient response of the nano-biosensor prototype to accurately follow the various steps of the DNA-aptamer binding-regeneration cycle, we further leverage this holistic approach for label-free, ultrasensitive drug detection, considering TFV, an antiviral drug for HIV treatment, as a model of drugs for this case study.

The average voltage difference with increasing TFV concentration is presented in Fig. 3. Solutions of TFV are prepared in the concentration range from 100 nM to 1 μ M. The detection is then performed for drug concentrations belonging within and slightly below the clinical range, providing the possibility for future applications with also diluted serum as well as ensuring economy of reagents, thus requiring a minimum amount of clinical samples.

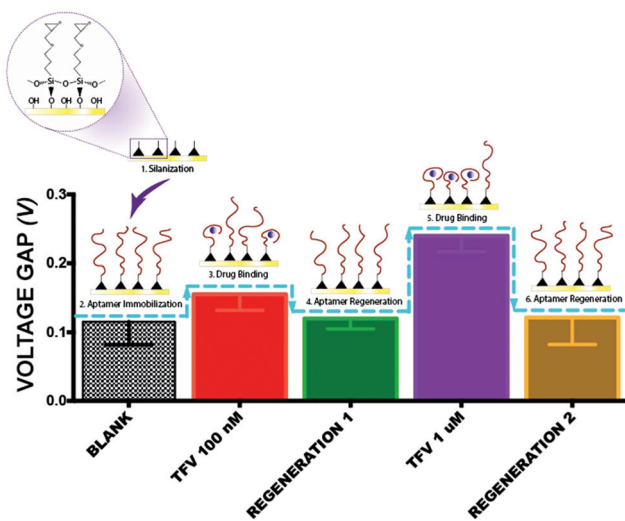


Fig. 2 DNA-aptamer immobilization, target molecule binding and DNA-aptamer regeneration cycle, illustrated through the electrical hysteresis variations.

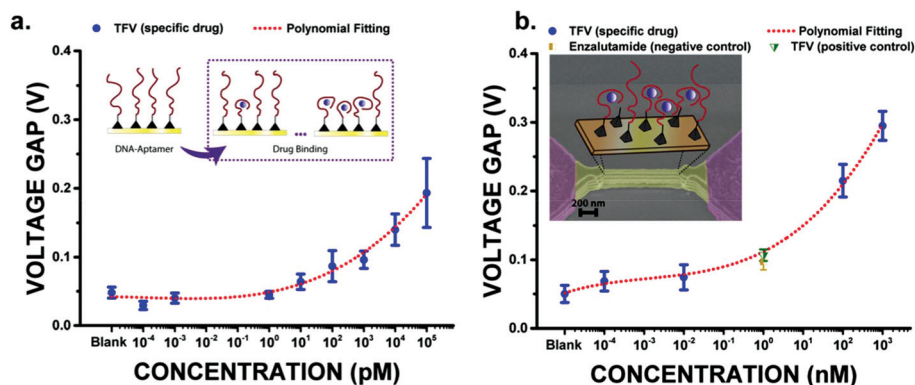


Fig. 3 Analytical performance and effective drug detection through the electrical hysteresis variations in buffer (a) and in full human serum (b).

To better show the performance of the proposed new biosensors, first, the TFV detection is proposed in Phosphate Buffer Saline (PBS) solutions as a proof of concept. Second, the effective drug detection in human serum is proposed in this paper too. All measurements are performed in air under controlled and stable ambient conditions (see the ESI†). In both cases, the successive uptake of negative charge at the nano-device surface leads to an increasing trend of the voltage gap that follows the increasing concentration of the detection target drug.

The average value obtained by nine independent nano-sensors indicates that a voltage gap of 29 ± 6 mV is first obtained for a concentration of 100 aM in buffer solution. An increasing trend of this parameter of the hysteresis is then depicted following the dose increase, as demonstrated in Fig. 3a until the value of 193 ± 51 mV for 100 nM, the highest concentration implemented for the case of buffer solution. In human serum, a hysteresis modification of 69 ± 38 mV is initially indicated for a concentration of 100 fM and reaches finally the value of 295 ± 61 mV for 1 μ M as shown in Fig. 3b. At the end of the complete dose response cycle in the human serum, a regeneration step is performed. Then the regenerated memristive aptasensor is anew exposed to an intermediate TFV concentration of 1 nM, the so-called “positive control” in order to further validate the consistency and effectiveness of the drug-detection methodology. It is depicted that the obtained voltage gap of 97 ± 31 mV actually fits within the values defined by the dose–response curve. This is a very important result that clearly demonstrates the efficiency of the proposed method and its applicability for continuous monitoring of therapeutic compounds as well. Moreover, the regeneration capability of the memristive aptasensor is also demonstrated in a real sample environment thanks to the regeneration step followed by the intermediate drug detection. This aspect is presented with more detail in ESI Fig. S3.† Furthermore, the implementation of a negative control drug, enzalutamide (a widely used anti-prostate cancer drug), at a concentration also equal to 1 nM is directly performed following the positive

control step. Indicatively, the 89 ± 35 mV voltage gap measured for the negative control actually coincides with the value obtained for the positive control bringing no significant hysteresis modification (<9% difference) with respect to the value obtained just before with the implementation of 1 nM concentration for the specific drug. Thus, it can be concluded that no drug binding occurs for the negative control case, exhibiting the specificity and selectivity of the methodology applied. The obtained calibration curves shown in Fig. 3 demonstrating the dose response for the specific target achieved follow indeed a typical polynomial fitting equation of third-order $y = \text{Intercept} + \alpha x^3 + \beta x^2 + \gamma x$, with a root-mean-square value (R -square) of 0.986, a Residual Sum of Squares (RSS) of 4.36×10^{-6} , an intercept of 49 ± 6 mV and coefficients $\alpha = 2.35041 \times 10^{-4} \pm 1.285 \times 10^{-4}$, $\beta = 0.00272 \pm 3.589 \times 10^{-4}$, and $\gamma = 0.0091 \pm 0.0027$, for buffer and a R -square of 0.99, a RSS of 0.19, an intercept of 112 ± 12 mV and coefficients $\alpha = 9.39543 \times 10^{-4} \pm 3.42 \times 10^{-4}$, $\beta = 0.0081 \pm 0.0016$, and $\gamma = 0.0291 \pm 0.003$, for human serum. A very low limit of detection (LOD) of 3.09 pM for PBS buffer and that of 1.38 nM for human serum are calculated from 9 independent samples following the method reported by Armbruster *et al.*³⁰ (ESI†). The hereby demonstrated LODs are compared with the state of the art, and they are highlighted as the best ever obtained, to the best of our knowledge, so far in the literature for drug detection in general, and for TFV in particular (Table 1).

The LOD presented here demonstrates 10 times higher sensitivity for the in-buffer drug detection with respect to the literature, and Table 1 shows twice better performance for drug sensing in human serum, ever obtained. The best case reported so far in human serum is mentioned in the work of Radhapyari *et al.*³¹ that reached 0.035 nM but in 10 times-diluted human serum, while we reached 1.38 nM in the undiluted one, which is much better. Thus, it is worth pointing out here that we worked with non-diluted human serum, further indicating the higher sensitivity and efficiency of our suggested methodology with respect to the best ever presented in the literature.

Table 1 State of the art list of reported drug detection to date

Target drug	Method	Surface	LOD (nM)		Linear range (nM)	Ref.	Comments
			Buffer	Bio-matrix			
6-Mercaptopurine	Voltam	Graphite/Polypyrrole/MWCNT	—	80	200–100 000	32	Diluted human urine sample
Gleevec	Conduc	Si-nanowire	—	—	Up to 100	33	—
Paracetamol	Voltam	MWCNT	2.9	—	5–1000	34	—
Penicillin	Voltam	Boron-doped diamond	—	320	400–100 000	35	Human urine sample
Tamoxifen	Voltam	Enzyme/Polyaniline/Pt	0.2	—	27–297	36	—
Clenbuteral	Voltam	Benzedithiol-GNPs	—	43.96	100–800	37	Diluted rat urine sample
Chloramphenicol	Ampero	Cds NPs/GNPs	0.14	—	0.15–2.94	38	—
Artesunate	Ampero	Gr-Polyaniline Nanocomposite	0.031	0.035	0.13–1	31	Highly diluted human serum
TFV	BSI	Glass chip	2.5	—	Up to 20	39	—
TFV	LC-MS	—	—	680	1360 to 350 000	40	Human urine
TFV	Voltam	HMDE	450	870	Up to 17 000	41	Diluted and precipitated human plasma
TFV	LC-UV	—	—	10.4	35 to 3480	42	—
TFV	LC-MS	—	—	7	35 to 3480	42	—
TFV	Memristive	Si-nanowire arrays	0.0031	1.38	0.001 to 1000	Present work	Full human serum

Voltam: voltammetry; Conduc: conductance; Ampero: amperometry; BSI: back scattering interferometry; LC: liquid chromatography; MS: mass spectroscopy; UV: ultraviolet; MWCNT: multiwalled carbon nanotubes; GNP: gold nanoparticle; HMDE: hanging mercury drop electrode.

Surface characterization

The alteration of the surface morphology of the device upon the consecutive treatment steps is a further proof of the applied bio-modification methodology efficiency. It is worth mentioning that the surface analysis is performed immediately after each modification step and no intermediate step or treatment is applied to the devices other than the treatment with the molecules of interest, leading to the heuristic conclusion that the morphology of the surface is clearly changed due to the reagents of interest that are indeed present on the nanostructure.

Of course, the variations of the nanodevice mean width measured after the different bio-modification steps throw light on the effective binding of the related molecules. Data analyzed considering several measures along the structure on different devices depict a mean increase of 3.25 ± 1.22 nm at the initial mean width of the structures for measurement performed upon the immobilization of DNA-aptamers on the silanized surface, while the mean width of 82.78 ± 1.08 nm is registered initially, just after silanization. This increase is compatible with the thickness of a layer of DNA-aptamer as registered immobilized on the Au surface with sizes in the range of 2.6–4.5 nm or 4.8–4.9 nm in salt and in aqueous solution, respectively.⁴³ In the literature, the aptamer height is also indicated with a value of 4–5 nm for an aptamer hairpin loop immobilized on DNA crossover tiles⁴⁴ and of 4.15 nm for DNA-aptamers bound on the surface of Si-NWs.⁴⁵ Then, according to the literature, the binding of large molecules such as proteins overall increases the height of the biological assay that is a well-expected consequence of the presence of large bio-molecules, for example proteases or proteins.^{44–47} Nevertheless, it is important to mention that an opposite effect has been

reported as well especially when uptaken molecules are very small for example adenosine.⁴³ This phenomenon is due to a change in aptamer conformation during the small molecule binding. Indeed, the mean width of the nanodevice appears decreased after the drug binding to the value of 84.08 ± 2.36 nm. The average difference after the drug binding of 1.95 ± 2.42 nm corresponds to the aptamer bending mainly due to the folding effect that follows the drug binding, taking into consideration the mean value of 86.03 ± 0.57 nm obtained after the aptamer immobilization. This value adheres in good approximation to the value reported in the literature for the DNA-aptamer conformational changes after the drug binding.⁴⁶ Namely, a comparison between the initial height for the unfolded DNA-aptamers of 4.8 nm and the height for the folded aptamer of 3.8 nm in the presence of adenosine, a small molecule in the size range of drugs, has been reported.⁴³ The case of unbound, unfolded but largely collapsed aptamers due to the presence of a salt solution is as well mentioned, and finally results in an average aptamer height of 2.6 nm.⁴³ These findings finally give an aptamer height difference in the range of 1 nm to 2.2 nm⁴³ after the exposure to the small molecules in salt containing solution.

In the present study, a combination of these phenomena occurs as well, a fact that is also demonstrated by the average mean width difference value upon the exposure of the device to the drug solution that indeed arises within the before-mentioned range (Fig. 4). Upon the device exposure to the drug solution, part of the DNA-aptamers is folded after successfully binding with the target drug. However, not all DNA-aptamers finally bind efficiently with the TFV, and, as a consequence, these aptamers remain unfolded or collapsed due to the presence of salts and positive substances that are included in the buffer or the serum solution. This phenomenon is well reflected

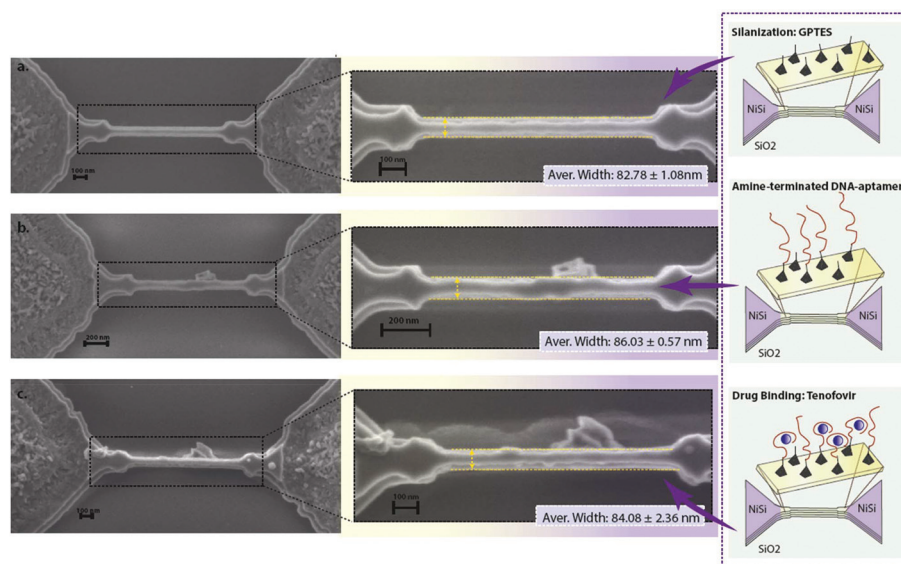


Fig. 4 SEM micrograph depicting the nanodevices anchored between the NiSi pads, which serve as electrical contacts of the freestanding nanostructures. The nanodevices are imaged directly after the silanization process (a), after the DNA-aptamer immobilization on the surface (b) as well as after exposure to TFV solution of 10 μ M. The mean width of the nanodevice changes accordingly, following the conditions introduced by each surface treatment.

through the standard error hereby presented. Namely, the value of the average difference varies from the height of the full standing aptamer on the silanized surface to the height of folded aptamers due to the drug binding that is the favorable behavior of the system, and finally in some cases to a completely collapsed system on the surface.

Conclusions

In the present work, a novel application of the memristive effect is presented for the first time, for detection of therapeutic compounds, through the coupling with the DNA-aptamer properties.

The hysteretic electrical characteristics exhibited by nanofabricated silicon nanowire-arrays, arising *via* surface treatment, are leveraged for successfully performing complete cycles of detection comprising DNA-aptamer immobilization, target binding, and DNA-aptamer regeneration. A successful label-free screening of TFV, used here, as a model drug and the case of study of any therapeutic compound are hereby demonstrated by achieving the best ever obtained LOD of 1.38 nM in drug monitoring applications in full human serum.

This novel approach holds great promise for the real-time continuous monitoring of therapeutic compounds that is a very important prospect of the suggested nano-biosensor in medical practices, particularly in the field of personalized medicine, which still lacks analytical methods for the continuous monitoring of low traces of drug species and therapeutic compounds.

Moreover, this paradigm can be expanded to detect a wide range of different molecules by accordingly choosing the corresponding aptamer-probes, and offer the potential for integration in more complex platforms for multiplexing configurations.

The present work, as a holistic approach, is of great significance in the field of label-free electrochemical nano-biosensors, boosting breakthrough applications in personalized medicine.

Author contributions

I. T. and N. A. contributed equally. S. C. led the research and conceived some experiments with I. T. and N. A. I. T. and N. A. performed all the fabrications, surface treatments, data acquisition, data analysis, and SEM imaging. I. T., N. A. and S. C. performed comparison with the literature. I. T. and N. A. have prepared the manuscript. S. C. gave suggestions on the manuscript. I. T., N. A., S. C., and G. D. M. have revised the manuscript.

Acknowledgements

The authors gratefully acknowledge the staff of the CMI Clean Room of EPFL and M. Zervas for technical advice regarding the nanofabrication process and P. Jolly for fruitful discussions concerning the aptamer regeneration. The authors acknowledge the financial support from the European Commission FP7 Programme through the Marie Curie Initial Training Network 'PROSENSE' (Grant No. 317420, 2012–2016) and by H2020-ERC-2014-ADG 669354 CyberCare.

References

- 1 E. A. Balant-Gorgia and L. P. Balant, Therapeutic Drug Monitoring, *CNS Drugs*, 2012, **4**, 432–453.
- 2 R. Weinshilboum and L. Wang, Pharmacogenomics: Bench to Bedside, *Nat. Rev. Drug Discovery*, 2004, **3**, 739–748.
- 3 D. H. J. Bunka and P. G. Stockley, Aptamers Come of Age – at Last, *Nat. Rev. Microbiol.*, 2006, **4**, 588–596.
- 4 F. Patolsky and C. M. Lieber, Nanowire Nanosensors, *Mater. Today*, 2005, **8**, 20–28.
- 5 G. Zheng, F. Patolsky, Y. Cui, W. U. Wang and C. M. Lieber, Multiplexed Electrical Detection of Cancer Markers with Nanowire Sensor Arrays, *Nat. Biotechnol.*, 2005, **23**, 1294–1301.
- 6 E. Stern, J. F. Klemic, D. A. Routenberg, P. N. Wyrembak, D. B. Turner-Evans, A. D. Hamilton, D. A. LaVan, T. M. Fahmy and M. A. Reed, Label-Free Immunodetection with CMOS-Compatible Semiconducting Nanowires, *Nature*, 2007, **445**, 519–522.
- 7 X. Duan, Y. Li, N. K. Rajan, D. A. Routenberg, Y. Modis and M. A. Reed, Quantification of the Affinities and Kinetics of Protein Interactions Using Silicon Nanowire Biosensors, *Nat. Nanotechnol.*, 2012, **7**, 401–407.
- 8 F. Patolsky, G. Zheng and C. M. Lieber, Fabrication of Silicon Nanowire Devices for Ultrasensitive, Label-Free, Real-Time Detection of Biological and Chemical Species, *Nat. Protoc.*, 2006, **1**, 1711–1724.
- 9 W. N. Frost, V. F. Castellucci, R. D. Hawkins and E. R. Kandel, Monosynaptic Connections Made by the Sensory Neurons of the Gill- and Siphon-Withdrawal Reflex in Aplysia Participate in the Storage of Long-Term Memory for Sensitization, *Proc. Natl. Acad. Sci. U. S. A.*, 1985, **82**, 8266–8269.
- 10 A. Lendlein and S. Kelch, Shape-Memory Polymers, *Angew. Chem., Int. Ed.*, 2002, **41**, 2034–2057.
- 11 J.-M. Lehn, From Supramolecular Chemistry towards Constitutional Dynamic Chemistry and Adaptive Chemistry, *Chem. Soc. Rev.*, 2007, **36**, 151–160.
- 12 J. Wu and R. L. McCreery, Solid-State Electrochemistry in Molecule/TiO₂ Molecular Heterojunctions as the Basis of the TiO₂ “Memristor”, *J. Electrochem. Soc.*, 2009, **156**, P29–P37.
- 13 Y. V. Pershin and M. D. Ventra, Memory Effects in Complex Materials and Nanoscale Systems, *Adv. Phys.*, 2011, **60**, 145–227.
- 14 L. O. Chua and S. M. Kang, Memristive Devices and Systems, *Proc. IEEE*, 1976, **64**, 209–223.
- 15 L. Chua, Resistance Switching Memories Are Memristors, *Appl. Phys. A*, 2011, **102**, 765–783.
- 16 L. O. Chua and S. M. Kang, Section-Wise Piecewise-Linear Functions: Canonical Representation, Properties, and Applications, *Proc. IEEE*, 1977, **65**, 915–929.
- 17 D. B. Strukov, G. S. Snider, D. R. Stewart and R. S. Williams, The Missing Memristor Found, *Nature*, 2008, **453**, 80–83.
- 18 T. Berzina, A. Smerieri, M. Bernabò, A. Pucci, G. Ruggeri, V. Erokhin and M. P. Fontana, Optimization of an Organic Memristor as an Adaptive Memory Element, *J. Appl. Phys.*, 2009, **105**, 124515.
- 19 D. I. Son, T. W. Kim, J. H. Shim, J. H. Jung, D. U. Lee, J. M. Lee, W. I. Park and W. K. Choi, Flexible Organic Bistable Devices Based on Graphene Embedded in an Insulating Poly(methyl Methacrylate) Polymer Layer, *Nano Lett.*, 2010, **10**, 2441–2447.
- 20 J. J. Yang, D. B. Strukov and D. R. Stewart, Memristive Devices for Computing, *Nat. Nanotechnol.*, 2013, **8**, 13–24.
- 21 J. J. Yang, M. D. Pickett, X. Li, D. A. A. Ohlberg, D. R. Stewart and R. S. Williams, Memristive Switching Mechanism for Metal/Oxide/Metal Nanodevices, *Nat. Nanotechnol.*, 2008, **3**, 429–433.
- 22 J. Borghetti, G. S. Snider, P. J. Kuekes, J. J. Yang, D. R. Stewart and R. S. Williams, “Memristive” Switches Enable “stateful” Logic Operations via Material Implication, *Nature*, 2010, **464**, 873–876.
- 23 P. J. Kuekes, D. R. Stewart and R. S. Williams, The Crossbar Latch: Logic Value Storage, Restoration, and Inversion in Crossbar Circuits, *J. Appl. Phys.*, 2005, **97**, 34301.
- 24 T. Tuma, A. Pantazi, M. Le Gallo, A. Sebastian and E. Eleftheriou, Stochastic Phase-Change Neurons, *Nat. Nanotechnol.*, 2016, **11**, 693–699.
- 25 M. D. Pickett, G. Medeiros-Ribeiro and R. S. Williams, A Scalable Neuristor Built with Mott Memristors, *Nat. Mater.*, 2013, **12**, 114–117.
- 26 T. Ohno, T. Hasegawa, T. Tsuruoka, K. Terabe, J. K. Gimzewski and M. Aono, Short-Term Plasticity and Long-Term Potentiation Mimicked in Single Inorganic Synapses, *Nat. Mater.*, 2011, **10**, 591–595.
- 27 D. Kuzum, R. G. D. Jeyasingh, B. Lee and H.-S. P. Wong, Nanoelectronic Programmable Synapses Based on Phase Change Materials for Brain-Inspired Computing, *Nano Lett.*, 2012, **12**, 2179–2186.
- 28 S. H. Jo, T. Chang, I. Ebong, B. B. Bhadviya, P. Mazumder and W. Lu, Nanoscale Memristor Device as Synapse in Neuromorphic Systems, *Nano Lett.*, 2010, **10**, 1297–1301.
- 29 I. Tzouvaradaki, P. Jolly, X. Lu, S. Ingebrandt, G. De Micheli, P. Estrela and S. Carrara, Label-Free Ultrasensitive Memristive Aptasensor, *Nano Lett.*, 2016, **16**, 4472–4476.
- 30 D. A. Armbruster and T. Pry, Limit of Blank, Limit of Detection and Limit of Quantitation, *Clin. Biochem. Rev.*, 2008, **29**, S49–S52.
- 31 K. Radhapyari, P. Kotoky, M. R. Das and R. Khan, Graphene–polyaniline Nanocomposite Based Biosensor for Detection of Antimalarial Drug Artesunate in Pharmaceutical Formulation and Biological Fluids, *Talanta*, 2013, **111**, 47–53.
- 32 H. Karimi-Maleh, F. Tahernejad-Javazmi, N. Atar, M. L. Yola, V. K. Gupta and A. A. Ensafi, A Novel DNA Biosensor Based on a Pencil Graphite Electrode Modified with Polypyrrole/Functionalized Multiwalled Carbon Nanotubes for Determination of 6-Mercaptopurine Anticancer Drug, *Ind. Eng. Chem. Res.*, 2015, **54**, 3634–3639.

- 33 W. U. Wang, C. Chen, K. Lin, Y. Fang and C. M. Lieber, Label-Free Detection of Small-Molecule-protein Interactions by Using Nanowire Nanosensors, *Proc. Natl. Acad. Sci. U. S. A.*, 2005, **102**, 3208–3212.
- 34 R. N. Goyal, V. K. Gupta and S. Chatterjee, Voltammetric Biosensors for the Determination of Paracetamol at Carbon Nanotube Modified Pyrolytic Graphite Electrode, *Sens. Actuators, B*, 2010, **149**, 252–258.
- 35 L. Švorc, J. Sochr, P. Tomčík, M. Rievaj and D. Bustin, Simultaneous Determination of Paracetamol and Penicillin V by Square-Wave Voltammetry at a Bare Boron-Doped Diamond Electrode, *Electrochim. Acta*, 2012, **68**, 227–234.
- 36 K. Radhapyari, P. Kotoky and R. Khan, Detection of Anticancer Drug Tamoxifen Using Biosensor Based on Polyaniline Probe Modified with Horseradish Peroxidase, *Mater. Sci. Eng., C*, 2013, **33**, 583–587.
- 37 B. Bo, X. Zhu, P. Miao, D. Pei, B. Jiang, Y. Lou, Y. Shu and G. Li, An Electrochemical Biosensor for Clenbuterol Detection and Pharmacokinetics Investigation, *Talanta*, 2013, **113**, 36–40.
- 38 D.-M. Kim, M. A. Rahman, M. H. Do, C. Ban and Y.-B. Shim, An Amperometric Chloramphenicol Immunosensor Based on Cadmium Sulfide Nanoparticles Modified-Dendrimer Bonded Conducting Polymer, *Biosens. Bioelectron.*, 2010, **25**, 1781–1788.
- 39 M. N. Kammer, I. R. Olmsted, A. K. Kussrow, M. J. Morris, G. W. Jackson and D. J. Bornhop, Characterizing Aptamer Small Molecule Interactions with Backscattering Interferometry, *Analyst*, 2014, **139**, 5879–5884.
- 40 M. Simiele, C. Carcieri, A. De Nicolò, A. Ariaudo, M. Sciandra, A. Calcagno, S. Bonora, G. Di Perri and A. D'Avolio, A LC-MS Method to Quantify Tenofovir Urinary Concentrations in Treated Patients, *J. Pharm. Biomed. Anal.*, 2015, **114**, 8–11.
- 41 R. Jain and R. Sharma, Cathodic Adsorptive Stripping Voltammetric Detection and Quantification of the Antiretroviral Drug Tenofovir in Human Plasma and a Tablet Formulation, *J. Electrochem. Soc.*, 2013, **160**, H489–H493.
- 42 M. E. Barkil, M.-C. Gagnieu and J. Guitton, Relevance of a Combined UV and Single Mass Spectrometry Detection for the Determination of Tenofovir in Human Plasma by HPLC in Therapeutic Drug Monitoring, *J. Chromatogr., B: Biomed. Appl.*, 2007, **854**, 192–197.
- 43 W. Zhao, W. Chiuman, J. C. F. Lam, S. A. McManus, W. Chen, Y. Cui, R. Pelton, M. A. Brook and Y. Li, DNA Aptamer Folding on Gold Nanoparticles: From Colloid Chemistry to Biosensors, *J. Am. Chem. Soc.*, 2008, **130**, 3610–3618.
- 44 Y. Liu, C. Lin, H. Li and H. Yan, Aptamer-Directed Self-Assembly of Protein Arrays on a DNA Nanostructure, *Angew. Chem., Int. Ed.*, 2005, **117**, 4407–4412.
- 45 K. S. Kim, H.-S. Lee, J.-A. Yang, M.-H. Jo and S. K. Hahn, The Fabrication, Characterization and Application of Aptamer-Functionalized Si-Nanowire FET Biosensors, *Nanotechnology*, 2009, **20**, 235501.
- 46 M. Godonoga, T.-Y. Lin, A. Oshima, K. Sumitomo, M. S. L. Tang, Y.-W. Cheung, A. B. Kinghorn, R. M. Dirkzwager, C. Zhou, A. Kuzuya, *et al.*, A DNA Aptamer Recognising a Malaria Protein Biomarker Can Function as Part of a DNA Origami Assembly, *Sci. Rep.*, 2016, **6**, 21266.
- 47 S. Song, L. Wang, J. Li, C. Fan and J. Zhao, Aptamer-Based Biosensors, *TrAC, Trends Anal. Chem.*, 2008, **27**, 108–117.
- 48 G. L. Witucki, A Silane Primer: Chemistry and Applications of Alkoxy Silanes, *J. Coat. Technol.*, 1993, **65**, 57–57.